Title

hNOA1 interacts with complex I and DAP3 and regulates mitochondrial respiration and apoptosis.

Journal

The Journal of biological chemistry, 284(8)

ISSN

0021-9258

Authors

Tang, Tingdong
Zheng, Bin
Chen, Sheng-Hong
et al.

Publication Date

2009-02-20

Peer reviewed

THE JOURNAL OF BIOLOGICAL CHEMISTRY VOL. 284, NO. 8, pp. 5414–5424, February 20, 2009

hNOA1 Interacts with Complex I and DAP3 and Regulates Mitochondrial Respiration and Apoptosis*[S]

Received for publication, October 9, 2008, and in revised form, December 15, 2008 Published, JBC Papers in Press, December 22, 2008, DOI 10.1074/jbc.M807797200

Tingdong Tang[‡], Bin Zheng[‡1], Sheng-hong Chen[‡§], Anne N. Murphy[¶], Krystyna Kudlicka[‡], Huilin Zhou[‡§], and Marilyn G. Farquhar[‡2]

From the Departments of [‡]Cellular and Molecular Medicine and [¶]Pharmacology and [§]Ludwig Institute for Cancer Research, University of California, San Diego, La Jolla, California 92093-0651

Mitochondria are dynamic organelles that play key roles in metabolism, energy production, and apoptosis. Coordination of these processes is essential to maintain normal cellular functions. Here we characterized hNOA1, the human homologue of AtNOA1 (*Arabidopsis thaliana* nitric oxide-associated protein 1), a large mitochondrial GTPase. By immunofluorescence, immunoelectron microscopy, and mitochondrial subfractionation, endogenous hNOA1 is localized within mitochondria where it is peripherally associated with the inner mitochondrial membrane facing the mitochondrial matrix. Overexpression and knockdown of hNOA1 led to changes in mitochondrial shape implying effects on mitochondrial dynamics. To identify the interaction partners of hNOA1 and to further understand its cellular functions, we performed immunoprecipitation-mass spectrometry analysis of endogenous hNOA1 from enriched mitochondrial fractions and found that hNOA1 interacts with both Complex I of the electron transport chain and DAP3 (death-associated protein 3), a positive regulator of apoptosis. Knockdown of hNOA1 reduces mitochondrial O_2 consumption ~20% in a Complex I-dependent manner, supporting a functional link between hNOA1 and Complex I. Moreover, knockdown of hNOA1 renders cells more resistant to apoptotic stimuli such as γ-interferon and staurosporine, supporting a role for hNOA1 in regulating apoptosis. Thus, based on its interactions with both Complex I and DAP3, hNOA1 may play a role in mitochondrial respiration and apoptosis.

Emerging evidence indicates that mitochondrial metabolism, apoptosis, and dynamics (fission and fusion) are closely intertwined. Apoptosis and changes in metabolism are associated with morphological changes in mitochondria (1, 2). Conversely, when mitochondrial morphology is altered either by mutations or altered expression of mitochondrial fission or fusion proteins such as the dynamin like large G proteins Drp1 and Opa1, the cell's susceptibility to apoptotic agents (3) or ability to generate ATP (4, 5) is altered.

Apoptosis is controlled by a diverse range of cell signals, which may originate either extracellularly (extrinsic inducers) or intracellularly (intrinsic inducers), and mitochondria play central roles in both pathways (6). The apoptotic pathways involve a growing list of mitochondria-associated proteins, such as Bad, cytochrome *c*, Smac, AIF, Bcl-2, and others, most of which are located either on the outer mitochondrial membrane (OMM)[3] or in the intermembrane space (IMS) (7). Recently, proteins of the mitochondrial matrix such as DAP3, have also been shown to be involved in apoptosis (8). DAP3 has been reported to be involved in both γ-interferon- (9) and tumor necrosis factor-α-induced (10) apoptosis as well as staurosporine-induced mitochondrial fragmentation (11), but the detailed mechanisms involved remain to be elucidated.

Besides their role in apoptosis, much more is known about the functions of mitochondria in respiration and generation of ATP. The electron transport chain in the inner mitochondrial membrane (IMM) contains four major enzyme complexes (Complexes I, II, III, and IV) that are involved in transferring electrons from NADH (Complex I-linked) or FADH2 (Complex II-linked) to O_2 and in pumping protons out of the matrix to create an electrochemical proton gradient, which is harnessed by ATP synthase to make ATP (12).

Despite the accumulating evidence showing intercommunication between mitochondrial metabolism, apoptosis, and dynamics, how these processes are coordinated remains to be elucidated. In this study we characterize hNOA1, the human homologue of *Arabidopsis thaliana* nitric oxide-associated protein, 1 (AtNOA1) (13). hNOA1 is a large G protein closely related to dynamin that is associated with the IMM. Perturbation of hNOA1 affects mitochondrial morphology, Complex I-linked O_2 consumption, and the cell's susceptibility to apoptotic stimuli, possibly through interactions with proteins such as Complex I and DAP3.

* This work was supported, in whole or in part, by National Institutes of Health Grants CA100768 and DKI7780 (to M. G. F.). The costs of publication of this article were defrayed in part by the payment of page charges. This article must therefore be hereby marked "*advertisement*" in accordance with 18 U.S.C. Section 1734 solely to indicate this fact.

[S] The on-line version of this article (available at http://www.jbc.org) contains supplemental Fig. S1.

[1] Present address: Division of Signal Transduction, Beth Israel Deaconess Medical Center; Dept. of Systems Biology, Harvard Medical School, Boston, MA 02215.

[2] To whom correspondence should be addressed: University of California, San Diego, George Palade Laboratories for Cellular and Molecular Medicine, Rm. 210, 9500 Gilman Drive, La Jolla, CA 92093-0651. Tel.: 858-534-7711; Fax: 858-534-8549; E-mail: mfarquhar@ucsd.edu.

[3] The abbreviations used are: OMM, outer mitochondrial membrane; PFA, paraformaldehyde; IMS, intermembrane space; AtNOA1, *A. thaliana* nitric oxide-associated protein 1; GST, glutathione *S*-transferase; siRNA, small interference RNA; RNAi, RNA interference; PBS, phosphate-buffered saline; BSA, bovine serum albumin; DMEM, Dulbecco's modified Eagle's medium; TUNEL, terminal deoxynucleotidyl transferase-mediated dUTP nick end labeling; IP-MS, immunoprecipitation-mass spectrometry; NOS, nitric-oxide synthase.

EXPERIMENTAL PROCEDURES

Vectors—Human hNOA1 (NP_115689) and human DAP3 (NP_004623) in pOTB7 cloning vector were purchased from Open Biosystems (Huntsville, AL). hNOA1 or its truncation mutants were subcloned by PCR using pOTB7-hNOA1 as a template into pET28a(+) (Novagen), pGEX-KG (GE), and pcDNA3.1/zeo(+) (Invitrogen) vectors. DAP3 was subcloned by PCR into pcDNA3.1/zeo(+) and pET28a(+) vectors. Sequences were verified by sequencing (DNA Sequencing Shared Resource, University of California at San Diego, Moores Cancer Center).

Antibodies—Antiserum against human hNOA1 was raised in rabbits against the purified His_6-tagged C terminus (amino acids 67–698) of human hNOA1 and affinity purified on GST-tagged hNOA1 coupled to CNBr-Sepharose 4B (Amersham Biosciences) as previously described (14). Bound anti-hNOA1 IgG was eluted with 0.2 M glycine, HCl, pH 2.5, and neutralized immediately with 1 M Tris. Other antibodies were obtained from the following sources: monoclonal antibodies against actin (Sigma-Aldrich), DAP3, and cytochrome *c* (BD Biosciences), ATP synthase and Complex I (Invitrogen), PDI (StressGen, MI), COX I (Mitosciences, OR), and mtHSP70 (Affinity BioReagents, CO). Polyclonal anti-PMP70 and Mrp-S27 IgG were purchased from Zymed Laboratories Inc. (South San Francisco, CA) and Novus Biologicals (Littleton, CO).

RNA Interference—The following small interfering RNA (siRNA) oligonucleotides synthesized by Sigma-Aldrich were used for RNAi knockdown of hNOA1: hNOA1-sense, 5′-GCA UGG UUA UGU CGU AGG AdTdT-3′; hNOA1-antisense, 5′-UCC UAC GAC AUA ACC AUG CdTdT-3′; DAP3-sense, 5′-CCA GGU UCC AGU UGA GAG UdTdT-3′; DAP3-antisense, 5′-ACU CUC AAC UGG AAC CUG GdTdT-3′. All oligonucleotides were designed based on human sequences. Scrambled RNA oligonucleotides (scramble II duplex, Dharmacon Research, CO) were used as controls. ~25,000 HeLa cells per well were seeded in 12-well plates. 24 h later, cells were transfected with 2 μl of 50 μM siRNA duplex and 3 μl of Oligofectamine (Invitrogen) per well. 72 h after transfection, cells were either fixed in 2% paraformaldehyde (PFA) for immunofluorescence or lysed directly on the plates with 2× Laemmli sample buffer for SDS-PAGE followed by immunoblotting.

Preparation of Tissue Lysates for Immunoblotting—Rat tissue fragments were minced into small pieces and homogenized with a Dounce homogenizer in homogenization buffer (PBS containing Complete protease inhibitor (Roche Applied Science)). Homogenates were solubilized in 1% Triton X-100 at 4 °C for 1 h with gentle rotation. Tissue lysates were prepared by centrifugation at 15,000 × *g* for 30 min (15). Protein concentrations were determined by BCA assay (Pierce). Proteins (~120 μg) from each tissue lysate were resolved by 10% SDS-PAGE, followed by immunoblotting with anti-hNOA1 IgG (15, 16).

Immunoblotting—Protein samples were resolved by 10% or 12% SDS-PAGE and transferred to polyvinylidene difluoride membranes (Millipore). Membranes were blocked with 5% nonfat milk in TBST (20 mM Tris-HCl, pH 7.5, 500 mM NaCl, 0.1% Tween 20) for 1 h at room temperature and incubated with 0.8 μg/ml affinity purified anti-hNOA1 IgG or other primary antibodies for 2 h at room temperature or overnight at 4 °C, followed by incubation with horseradish peroxidase-conjugated goat anti-rabbit IgG (Biodesign, 1:5000 in TBST containing 5% milk) or anti-mouse IgG (Bio-Rad, 1:3000 in TBST) for 1 h and detection by enhanced chemiluminescence (ECL) (Pierce).

[α-^{32}P]GTP Binding Assay—hNOA1 (amino acids 67–698) and full-length $G\alpha_{i3}$ were amplified by PCR and subcloned into pET28a(+) vector (Novagen). His_6-$G\alpha_{i3}$ and His_6-hNOA1-(67–698) fusion proteins were expressed in *Escherichia coli* BL21(DE3) (Stratagene), purified on nickel-nitrilotriacetic acid beads (Qiagen), and eluted with 75 mM imidazole according to the manufacturer's instructions. The protein concentration for each protein was determined by Bradford assay. Approximately 1.5 μg of the above fusion proteins and 1.5 μg of BSA were suspended in 17 μl of binding buffer (25 mM HEPES, 25 mM PIPES, pH 7.0, 2 mM $MgCl_2$, 90 mM NaCl), respectively. The reaction was started by adding 3 μl of 0.5 μM [α-^{32}P]GTP (3000 Ci/mmol, Amersham Biosciences) and incubated at room temperature for 5 min. The reaction mixture was subsequently placed on pre-chilled parafilm and irradiated in a UV Spectralinker™ 1800 (Spectrontics Corp.) at 254 nm for 5 min with samples 10 cm away from the UV lamp. After cross-linking, samples were resolved by SDS-PAGE, and the gel was stained with Coomassie Brilliant Blue (Sigma-Aldrich), destained and dried, followed by autoradiography on BioMax MR film (Eastman Kodak) (17, 18).

Cell Culture and Transfection—HEK293, COS7, and HeLa cells were maintained in Dulbecco's modified Eagle's high glucose medium (DMEM, Invitrogen) containing 10% fetal bovine serum (HyClone), penicillin, streptomycin, and glutamine (Invitrogen). COS7 and HeLa cells were transfected using FuGENE 6 (Roche Applied Science) according to the manufacturer's instructions.

Immunofluorescence—COS7 or HeLa cells were fixed in 2% PFA in 100 mM phosphate buffer, pH 7.4, for 40 min, permeabilized with 0.1% Triton X-100 for 10 min, and incubated with primary antibodies in 2% BSA for 1 h at room temperature, followed by Alexa Fluor 594-conjugated goat anti-mouse and/or Alexa 488 goat anti-rabbit $F(ab')_2$ (Molecular Probes) for 1 h. Specimens were analyzed using a Zeiss Axio Imager M1 equipped with a Hamamatsu Orca ER charge-coupled device (16). Images were processed as tiff files using Adobe Photoshop (Adobe Systems, San Jose, CA).

Immunogold Labeling—Rat kidneys were fixed overnight in 4% PFA/0.2% glutaraldehyde in 0.1 M phosphate buffer, pH 7.4, pelleted in 10% gelatin in phosphate buffer, cryoprotected, and snap frozen in liquid nitrogen. Ultrathin cryosections (70–90 nm) were cut at −100 °C on a Leica Ultracut UCT with an EM FCS cryoattachment (Leica, IL) using a glass knife (Diatome US), picked up with a 1:1 mixture of 2.3 M sucrose and 2% methyl cellulose (15 cp), and transferred onto Formvar- and carbon-coated copper grids. Sections were blocked and incubated with primary antibodies for 2 h at room temperature, followed by 5- or 10-nm gold conjugated to goat anti-rabbit IgG (Amersham Biosciences) for 1 h. Sections were contrasted in uranyl acetate in 1.8% methyl cellulose on ice. Grids were viewed and photographed using a Philips CM-10 transmission

electron microscope (FEI) equipped with a 794 Multiscan charge-coupled device camera (Gatan) (19).

Preparation of Rat Liver Mitochondria—Mitochondria were purified as described (20) with minor modifications. Fresh rat liver was minced, washed, and homogenized with 30–40 strokes of a tight-fitting Potter-Elvehjem homogenizer in 15 ml of ice-cold MSHE plus BSA buffer (210 mM mannitol, 70 mM sucrose, 5 mM HEPES, pH 7.4, with KOH, 2 mM EGTA, with 0.5% fatty-acid free BSA and Complete protease inhibitor (Roche Applied Science)). The homogenate was centrifuged (10 min at 600 × *g*) to remove nuclei and unbroken cells. The supernatant was collected and centrifuged again at 15,000 × *g* for 10 min to pellet the crude mitochondrial fraction, which was subsequently placed on top of a gradient of 35% Histodenz (Sigma-Aldrich), 17.5% Histodenz, and 6% Percoll (Sigma-Aldrich), followed by centrifugation at 19,000 rpm in an SW40 Ti rotor (Beckman) for 1 h. The purified mitochondrial fraction was collected from the 35% and 17.5% Histodenz interface, centrifuged at 15,000 × *g* for 15 min, and resuspended in a small volume of MSHE buffer.

Preparation of Mitochondria from HEK293 Cells—Preparation of mitochondria from HEK293 cells was similar to that for rat liver mitochondria with modifications. Briefly, cell pellets from 35 15-cm dishes of HEK293 cells were washed (2×) with MSHE plus BSA buffer and Complete protease inhibitor and suspended in 20 ml of the same buffer. Cells were homogenized with 10 strokes of a zero-clearance homogenizer (Kontes Glass Co.). The postnuclear supernatant was collected by centrifugation and centrifuged at 11,200 rpm to prepare a crude mitochondrial fraction. The pellet was washed twice with MSHE plus BSA buffer and once with MSHE buffer, and suspended in ~500 μl of MSHE buffer. Protein concentration was determined by Bradford assay, and the fractions were kept on ice until further use.

Mitochondrial Subfractionation—Approximately 150 μg of mitochondria freshly isolated from HEK293 cells was resuspended in 100 μl of hypotonic medium (10 mM KCl, 2 mM HEPES, pH 7.2) for 20 min on ice to swell mitochondria and break the OMM, thereby releasing the proteins from the IMS (21). The swollen mitochondria were subsequently centrifuged at 11,200 rpm to collect the supernatant (which contains the soluble IMS proteins) and the pellet, which was suspended in the same volume as the supernatant. Equal volumes of supernatant and pellet were separated by 12% SDS-PAGE, followed by immunoblotting with anti-hNOA1, anti-cytochrome *c*, anti-DAP3, and anti-Opa1 IgG.

For the trypsin digestion assay (22), trypsin (final concentration, 25 μg/ml) was added to swollen mitochondria for 20 min at room temperature. Digestion was stopped by adding soybean trypsin inhibitor (100 μg/ml), and the samples were immediately boiled for 5 min and separated by 12% SDS-PAGE. For the high salt or alkaline washes (22), a swollen mitochondrial pellet prepared as above was washed with either high salt buffer (200 mM KCl, 2 mM HEPES, pH 7.2) or alkaline solution (0.1 M Na_2CO_3, pH 11.5) for 10 min on ice. After washing, samples were centrifuged at 11,200 rpm. The supernatant and pellets were collected, and the pellet was resuspended in the same volume (100 μl) of MSHE. Laemmli sample buffer was added to the fractions, samples were boiled for 5 min, and the proteins were separated by 12% SDS-PAGE for immunoblotting.

hNOA1 Tet-on Inducible Stable COS7 Cells—Tet-on-inducible stable COS7 cells overexpressing hNOA1 were made using the RevTet System (Clontech) according to the manufacturer's instructions. Cells stably expressing hNOA1 were cultured in the presence or absence of 1 μg/ml doxycycline (Clontech) for 4 days to induce the expression of hNOA1. The induced cells were identified by immunostaining with anti-hNOA1 IgG, and mitochondria were immunostained with anti-cytochrome *c* IgG. In each experiment, 12 fields were randomly selected, and among the induced cells those with small, round mitochondria *versus* normal filamentous mitochondria were counted. Statistical analysis was performed by two-tailed Student's *t* test.

Immunoprecipitation and Mass Spectrometry—Approximately 1 mg of mitochondria prepared from HEK293 cells was lysed in 1% Triton X-100 in PBS containing Complete protease inhibitors for 30 min. After centrifugation at 13,000 × *g*, the supernatant was incubated with anti-hNOA1 or preimmune IgG (40 μg) for 4 h at 4 °C, followed by incubation with 30 μl of protein A-Sepharose CL-4B (Amersham Biosciences) for an additional 1 h at 4 °C. The beads were washed (3×) with lysis buffer and boiled in Laemmli sample buffer, and bound immune complexes were analyzed by 10% SDS-PAGE (19), stained with silver (Quest™ silver staining kit, Invitrogen), and the bands obtained in the hNOA1 immunoprecipitates were processed for protein identification by mass spectrometry as described previously (23, 24).

Co-Immunoprecipitation—HEK293 cell lysates were prepared as above in 1% Triton X-100 in PBS containing protease inhibitors (0.12 mg/ml phenylmethylsulfonyl fluoride, 2 mg/ml leupeptin, and 1 mg/ml aprotinin). Cell lysates were incubated with primary antibodies overnight at 4 °C, followed by incubation with protein A- or G-Sepharose (Calbiochem, San Diego, CA) for an additional 1 h at 4 °C. Beads were washed (3×) with lysis buffer and boiled in Laemmli sample buffer, and bound immune complexes were analyzed by SDS-PAGE and immunoblotting (19).

In Vitro Pulldown Assays—GST-hNOA1-(67–698) or GST fusion proteins were purified on glutathione-Sepharose 4B (Amersham Biosciences) as above. HEK293 cell lysates were prepared from a 10-cm confluent plate with 1% Triton X-100 in PBS, plus Complete protease inhibitor. [^{35}S]Met-labeled, *in vitro* translation products of DAP3 were prepared using the TnT T7 rabbit reticulocyte Quick Coupled Transcription/Translation system (Promega, Madison, WI) in the presence of [^{35}S]Met (>1000 Ci/mmol, PerkinElmer Life Sciences). His_6-DAP3 was expressed in BL21(DE3) cells (Stratagene) and purified on nickel-nitrilotriacetic acid-agarose affinity resin (Qiagen) according to the manufacturer's instructions. His_6-DAP3 fusion protein was eluted with 250 mM imidazole (Sigma-Aldrich). For pulldown assays, GST or GST-hNOA1-(67–698) fusion proteins (~2 μg) immobilized on beads were incubated with HEK293 cell lysate, *in vitro*-translated DAP3 or 200 ng of purified His_6-DAP3 in PBS with 1% Triton X-100 in the presence of Complete protease inhibitor for 3 h at 4 °C, and washed (3×) with the same buffer. Bound proteins were eluted with Laemmli sample

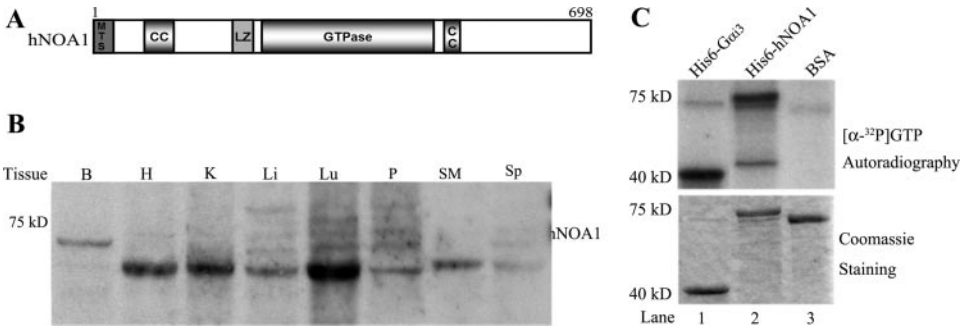

FIGURE 1. **hNOA1 is a large GTP-binding protein.** *A*, domain organization of human hNOA1. *MTS*, mitochondrial targeting sequence; *CC*, coiled coil; *LZ*, leucine zipper; *GTPase*, GTPase domain. *B*, immunoblot showing the expression of hNOA1 in rat tissues. hNOA1 is ubiquitously expressed in all tissues tested with slightly higher expression in heart (*H*), kidney (*K*), and lung (*Lu*) followed by skeletal muscle (*SM*) and liver (*Li*), and the lowest expression in pancreas (*P*) and spleen (*Sp*). In brain (*B*), a slightly higher band was detected. Equal aliquots (~120 μg of protein) of each tissue lysate were separated by 10% SDS-PAGE, transferred to polyvinylidene difluoride membranes, and immunoblotted with anti-hNOA1 IgG. *C*: *Upper panel*, hNOA1 binds [α-^{32}P]GTP *in vitro*. [α-^{32}P]GTP binds to His_6-Gα_{i3} (*lane 1*) and His_6-hNOA1 (*lane 2*), but not BSA (*lane 3*). The ~40-kDa band in *lane 2* is most likely a degradation product of His_6-hNOA1. Equal amounts (1.5 μg) of His_6-Gα_{i3}, His_6-hNOA1, and BSA shown by Coomassie Blue staining (*lower panel*) were incubated with [α-^{32}P]GTP (*upper panel*), followed by UV cross-linking, SDS-PAGE, and autoradiography.

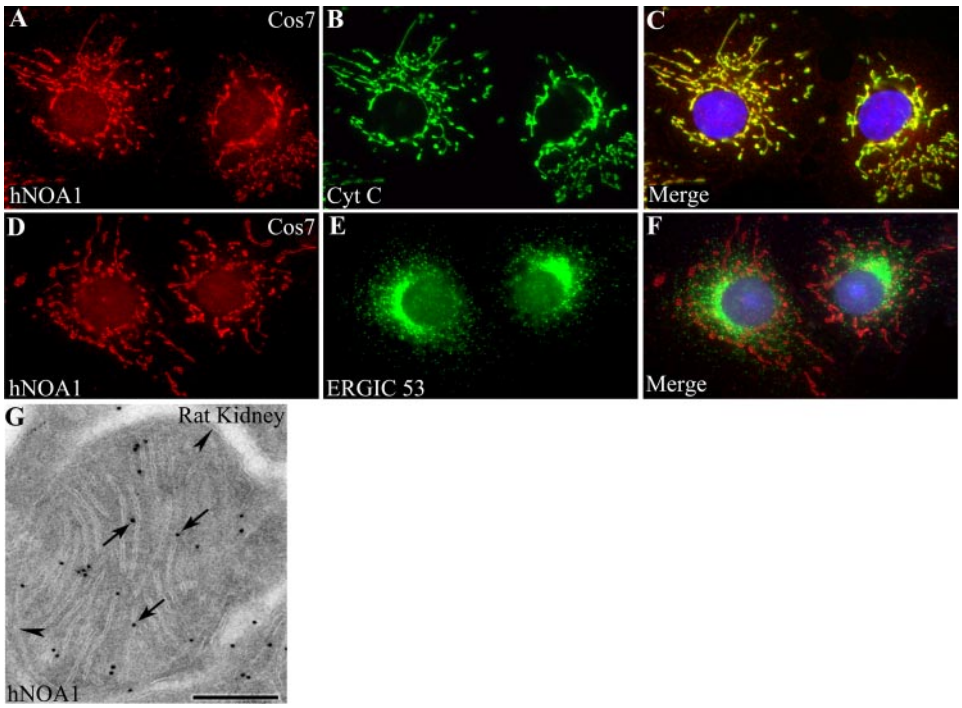

FIGURE 2. **Endogenous hNOA1 is localized on mitochondrial cristae.** *A–C*, immunofluorescence showing endogenous hNOA1 colocalizes with the mitochondrial marker cytochrome *c* (*Cyt C*) in COS7 cells (*yellow* in *merge image*). *D–F*, endogenous hNOA1 does not colocalize with the Golgi marker ERGIC-53. COS7 cells were fixed in 2% PFA and incubated with affinity-purified rabbit anti-hNOA1 IgG (1:500) and mouse anti-cytochrome *c* (1:1000) or anti-ERGIC-53 (1:250) IgG, followed by goat anti-rabbit Alexa Fluor-594 (1:500) and anti-mouse Alexa Fluor-488 (1:500) F(ab')$_2$, and examined by immunofluorescence. *G*, immunogold labeling demonstrating that hNOA1 is associated largely with the cristae (*arrows*) but not the OMM (*arrowheads*). Ultrathin cryosections of rat kidney were prepared as described under "Experimental Procedures" and labeled with anti-hNOA1 IgG followed by 10 nm gold, goat anti-rabbit IgG conjugates. *Bar* = 1 μm.

buffer and resolved by SDS-PAGE. For the *in vitro* [^{35}S]Met-labeled DAP3 pulldown assay, the gel was stained with Coomassie Brilliant Blue, destained, and dried, followed by autoradiography on Kodak BioMax MR film (19). For the HEK293 cell lysate and His_6-DAP3 pulldown assays, bound proteins were transferred to polyvinylidene difluoride membranes followed by immunoblotting with anti-Mrp-S27 and DAP3 IgG.

Measurement of O_2 Consumption on Digitonin-permeabilized Cells—HeLa cells were treated with control or hNOA1-specific siRNA for 3 days and then trypsinized and collected in DMEM. For measurement of respiration in permeabilized cells, 1.0×10^7 cells were centrifuged, resuspended in 0.6 ml of KCl medium (125 mM KCl, 2 mM K_2HPO_4, 20 mM HEPES, 1 mM $MgCl_2$, pH 7.0), transferred to the Hansatech Oxytherm electrode chamber (Hansatech Instruments, PP Systems, Amesbury, MA), and then permeabilized with 0.01% digitonin in the presence of 5 mM glutamate and 5 mM malate (Complex I-linked) or 5 mM succinate (Complex II-linked) in the presence of 2 μM rotenone as oxidizable substrates. After addition of 10 μg/μl oligomycin, maximal rates of electron flow through the electron transport chain (state 3_u) were subsequently measured by titration with the uncoupler carbonyl cyanide *p*-trifluoromethoxyphenylhydrazone (80 nM, Calbiochem) (25).

Cell Viability Assay—25,000 HeLa cells per well were plated in 12-well plates. 24 h after plating cells were transfected with control, hNOA1-specific, or DAP3-specific siRNA with Oligofectamine (Invitrogen). 12 h after transfection, the cell culture medium was changed to fresh DMEM with 1000 units/ml of γ-interferon for an additional 60 h. Cells were then trypsinized, collected in 1 ml of DMEM, and counted using a Vi-Cell cell counter (Beckman Coulter).

In Situ Cell Death Detection (TUNEL Staining)—HeLa cells transfected with control or hNOA1-specific siRNA for 3 days were treated with 2 μM staurosporine (Sigma-Aldrich) for different times. Cells were fixed in 2% PFA for 40 min, and TUNEL staining was carried out using the In Situ Cell Death Detection Kit TMR red (Roche Applied Science), followed by 4′,6-diamidino-2-phenylindole staining of nuclei.

RESULTS

hNOA1 Is a Large GTP-binding Protein—hNOA1, the human homologue of *A. thaliana* AtNOA1, is 698 amino acids

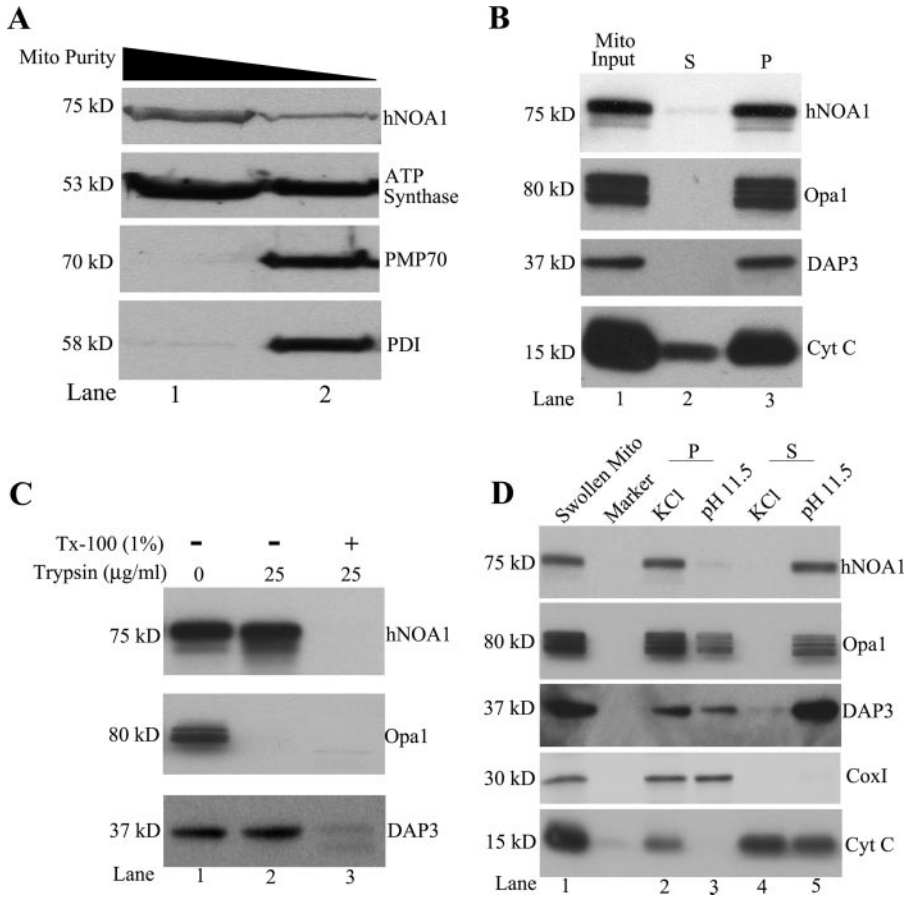

FIGURE 3. **hNOA1 is peripherally associated with the IMM facing the matrix.** *A*, hNOA1 and ATP synthase (mitochondrial marker) are enriched in purified rat liver mitochondria (*lane 1*), which lack PMP70 (peroxisome marker) and protein disulfide isomerase (*PDI*) (ER marker). PMP70 and PDI are detected in a crude mitochondrial fraction (*lane 2*). Mitochondria were prepared from rat liver by differential centrifugation and further enriched by Histodenz gradient centrifugation. ~20 μg of the crude (*lane 2*) and purified (*lane 1*) fractions were separated by 10% SDS-PAGE and immunoblotted for hNOA1, ATP synthase, PMP70, or PDI. *B*, hNOA1 is not released by mitochondrial swelling. hNOA1, Opa1, and DAP3 are found exclusively in the pellet (*P*) (*lane 3*), which contains proteins on or associated with the IMM and matrix. A fraction of the cytochrome *c* was released into the supernatant (*S*) with the soluble IMS proteins (*lane 2*) as expected. ~150 μg of mitochondria prepared from HEK293 cells by differential centrifugation were swollen with hypotonic medium to break the OMM, keeping the IMM intact. The swollen mitochondria were pelleted by centrifugation, the supernatant (*S*) containing the soluble proteins released from the IMS was collected, and the pellet (*P*) was suspended in the same volume as the supernatant. Equal volumes of supernatant and pellet were separated by 12% SDS-PAGE, followed by immunoblotting for hNOA1, cytochrome *c*, DAP3, and Opa1. *C*, hNOA1 and DAP3 are resistant to trypsin digestion, whereas Opa1 is susceptible to trypsin digestion of swollen mitochondria (*lane 2*). Digestion of Opa1 is expected based on its localization on the IMM facing the intermembrane space. After adding 1% Triton X-100, hNOA1, Opa1, and DAP3 are digested by trypsin (*lane 3*). Mitochondria, prepared and swollen as in *B*, were incubated with or without 25 μg/ml trypsin and/or 1% Triton X-100 for 20 min. After incubation, the trypsin activity was stopped by addition of soybean trypsin inhibitor, and samples were immunoblotted for hNOA1, DAP3, and Opa1. *D*, hNOA1 is extracted by sodium carbonate (pH 11.5), but not by high salt (KCl). hNOA1, Opa1, and DAP3 remain in the pellet (*P*) after the high salt (KCl) wash (*lane 2*), but are extracted and released into the supernatant (*S*) after sodium carbonate treatment (pH 11.5, *lane 3*). As a control, cytochrome *c* can be extracted by both high salt (KCl) and sodium carbonate (pH 11.5) treatment (compare *lanes 4* and *5* with *lanes 2* and *3*). COX I, an integral membrane protein, remains in the pellet after high salt or sodium carbonate (pH 11.5) treatment (*lanes 2* and *3*). A swollen mitochondrial pellet prepared as in *B*, was suspended and washed in either high salt or sodium carbonate (200 mM KCl) as described under "Experimental Procedures." After extraction, the suspension was centrifuged to yield the supernatant (*S*) and pellet (*P*), which was suspended in the same volume as the supernatant. An equal volume of each fraction was immunoblotted for hNOA1, Opa1, DAP3, Cox I, and cytochrome *c*.

with a predicted molecular mass of 78 kDa. hNOA1 contains a mitochondrial targeting sequence, two coiled-coil regions, a leucine zipper, and a GTPase domain (Fig. 1*A*). hNOA1 is highly conserved through evolution from prokaryotes to eukaryotes, especially within the GTP-binding domain (18). The *Arabidopsis* homologue of hNOA1 was originally identified as a mitochondrial NOS (nitric-oxide synthase) and named AtNOS1 based on its sequence homology to *Helix pomatia* NOS (26, 27). Although the *Arabidopsis* NOS1 mutant was shown to be impaired in NO (nitric oxide) synthesis, it has been controversial whether the recombinant AtNOS1 protein or its ortholog purified from *Escherichia coli* are able to catalyze NOS reactions *in vitro* (28, 29). Consequently, it was suggested that AtNOS1 be renamed to AtNOA1 for NO associated protein in *A. thaliana* (30).

To examine the tissue distribution of hNOA1, we generated an affinity-purified rabbit polyclonal antibody against hNOA1 and performed immunoblotting on rat tissue lysates. As shown in Fig. 1*B*, we found that hNOA1 is ubiquitously expressed in all tissues tested, with slightly higher expression in heart, kidney, and lung, lower expression in brain, liver, and skeletal muscle, and lowest expression in pancreas and spleen. In brain, a slightly higher molecular weight band was observed than in other tissues.

To test whether hNOA1 is indeed a GTP-binding protein, we performed an [α-^{32}P]GTP binding assay and found that both His_6-hNOA1 and His_6-Gα_{i3} (used as a positive control) bind [α-^{32}P]GTP (Fig. 1*C*), whereas BSA (negative control) did not bind under the same conditions, suggesting that hNOA1 is a *bona fide* GTP-binding protein.

Endogenous hNOA1 Is Localized in Mitochondria—The V5-tagged mouse homologue of hNOA1 was shown previously to be localized in mitochondria when expressed in COS1 cells (30). To examine the localization of endogenous hNOA1, we used affinity-purified anti-hNOA1 IgG and performed double labeling for hNOA1 and cytochrome *c*, a mitochondrial marker, ERGIC 53, a *cis*-Golgi marker (31), and LAMP2, a lysosomal marker (32). We found that staining for endogenous hNOA1 overlapped with cytochrome *c* (Fig. 2, *A–C*) but not with ERGIC 53 (Fig. 2, *D–F*) or LAMP2 (data not shown). We confirmed the mitochondrial localization of hNOA1 by co-immunostaining with two additional mitochondrial markers (ATP synthase and Complex I) in HeLa, Clone 9, and HEK293 cells (data not shown).

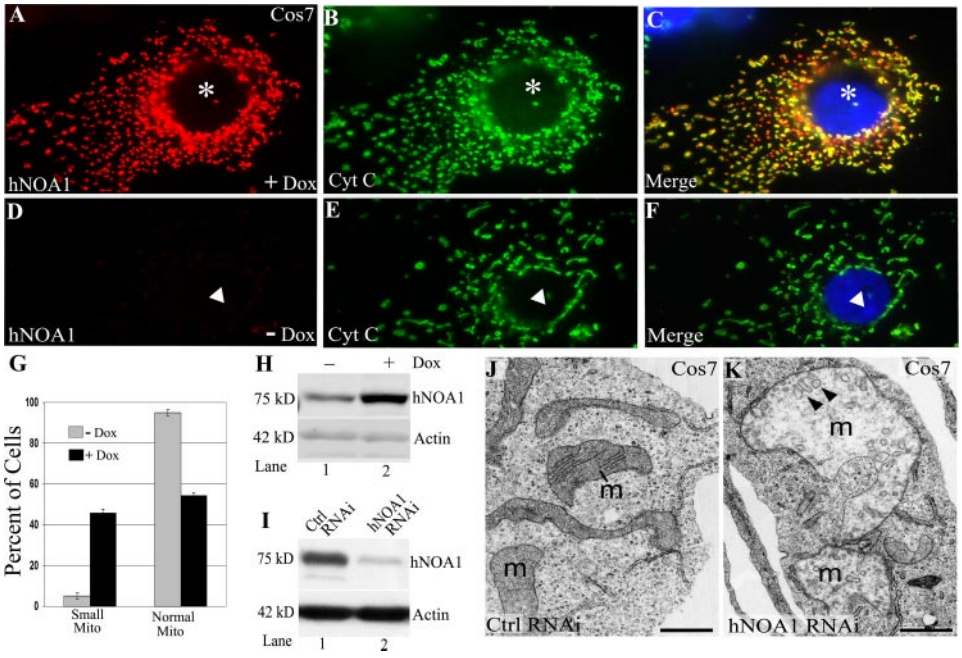

FIGURE 4. **Changes in hNOA expression affect mitochondrial dynamics.** *A–C*, in COS7 cells with high levels of hNOA1 expression (*asterisk*), mitochondria as marked by cytochrome *c* (*Cyt C*) staining often become small and round. *D–F*, in uninduced cells (*triangles*) mitochondria are more filamentous (see also Fig. 2, *A–C*). Tet-on hNOA1-inducible stable COS7 cells were treated or not with 1 μg/ml doxycycline for 4 days, followed by fixation and immunofluorescence as in Fig. 2, *A–C*. *G*, in control COS7 cells (−*DOX*), ~95% of the cells show normal filamentous mitochondria and <5% have small round mitochondria. After induction of hNOA1 expression (+*DOX*), ~41% of the cells show small round mitochondria. 20,000 Tet-on hNOA1-inducible stable COS7 cells were plated per well in 12-well plates with or without 1 μg/ml doxycycline for 4 days. Cells were fixed and processed for immunofluorescence with anti-hNOA1 and anti-cytochrome *c* IgG. The total number of cells in 12 randomly selected fields (250 for +*Dox*; 338 for −*Dox*) were counted based on 4′,6-diamidino-2-phenylindole nuclear staining, and those with small and round mitochondria were counted. *H*, immunoblot showing that hNOA1 is efficiently induced after addition of 1 μg/ml doxycycline (+*Dox*) for 4 days. hNOA1 Tet-on-inducible COS7 cells plated in 12-well plates were treated with (+*Dox*) (*lane 2*) or without (−*Dox*) (*lane 1*) doxycycline for 4 days. After induction, cells were lysed directly on the plate with 2× sample buffer followed by 10% SDS-PAGE and immunoblotting with anti-hNOA1 and anti-actin IgG. *I*, immunoblot showing that hNOA1 is efficiently depleted by siRNA specific for hNOA1. COS7 cells were transfected with control (*lane 1*) or hNOA1-specific siRNA (*lane 2*) using Oligofectamine. After 3 days of transfection, cells were lysed directly in sample buffer, followed by immunoblotting with anti-hNOA1 and anti-actin IgG. *J* and *K*, COS7 cells were similarly transfected with control (*J*) or hNOA1-specific (*K*) siRNA and examined by electron microscopy. In cells transfected with hNOA1 siRNA, the mitochondria (*m*) appear larger, and the mitochondrial matrix has a lower density than in controls. *Bar* = 1 μm.

To investigate the mitochondrial localization of hNOA1 at higher resolution, we carried out immunogold labeling of endogenous hNOA1 using affinity-purified anti-hNOA1 IgG on ultrathin cryosections of rat kidney tissue. By electron microscopy, gold particles were found predominantly inside mitochondria where they were closely associated with the mitochondrial cristae, but few or no gold particles were seen on the OMM (Fig. 2*G*). These results confirm the localization of hNOA1 in mitochondria and suggest its association with the IMM, IMS, or mitochondrial matrix, but not the OMM.

hNOA1 Is Enriched in Purified Rat Liver Mitochondria—To obtain biochemical confirmation of the distribution of hNOA1 in mitochondria, we prepared mitochondrial fractions from rat liver by differential centrifugation followed by Histodenz gradient centrifugation. The purity of mitochondria was monitored by enrichment of ATP synthase and absence of peroxisomal (PMP70) and ER (PDI) markers. hNOA1 as well as ATP synthase were found to be enriched (2- to 3-fold) in the purified mitochondrial fraction compared with fractions prepared by differential centrifugation (Fig. 3*A*). Collectively, the results obtained by immunofluorescence, immunoelectron microscopy, and cell fractionation establish that endogenous hNOA1 is a *bona fide* mitochondrial protein.

hNOA1 Is Localized on the Matrix Side of the IMM—To pinpoint the specific mitochondrial subcompartment in which hNOA1 is located, we carried out mitochondrial subfractionation. Mitochondrial fractions prepared from HEK293 cells by differential centrifugation were swollen in hypotonic medium, which releases the content of the IMS. We found that a fraction of the cytochrome *c* (which is present both in the IMS and on the IMM facing the IMS (33, 34)) was released into the supernatant by this treatment (Fig. 3*B*). hNOA1, together with DAP3 (located on the matrix side of the IMM (8)) and Opa1 (a peripheral membrane protein associated with the IMM facing the IMS (35)) remained in the pellet (Fig. 3*B*). To further investigate the topology of hNOA1, we carried out trypsin digestion on swollen mitochondria. We found that, as expected, Opa1 (located on the IMM facing the IMS) was completely digested when trypsin was added to the swollen mitochondria, whereas hNOA1 and DAP3 (located on the IMM facing the matrix) were protected from trypsin digestion (Fig. 3*C*). These data indicate that hNOA1 is associated either with the inner surface of the IMM facing the matrix or the mitochondrial matrix.

To determine which is the case, we performed high salt (200 mM KCl) or high pH (sodium carbonate, pH 11.5) extraction on a swollen mitochondrial pellet and found that hNOA1, Opa1, and DAP3 were extracted by sodium carbonate, but not by high salt (Fig. 3*D*). Cytochrome *c* was extracted by both high salt and sodium carbonate (21). The integral membrane protein COX I (cytochrome *c* oxidase, subunit 1), remained in the pellet after high salt or sodium carbonate extraction as expected. From these results we conclude that hNOA1 is a peripheral membrane protein that is tightly bound to the IMM. This is consistent with the fact that it lacks a putative transmembrane domain based on amino acid sequence. From these data together with the results from trypsin digestion, we conclude that hNOA1 is peripherally anchored to the IMM facing the matrix.

Overexpression or Depletion of hNOA1 Affects Mitochondrial Morphology—To further investigate the role of hNOA1 in mitochondria, we generated Tet-on-inducible COS7 cells stably expressing hNOA1. We found that, after inducing expres-

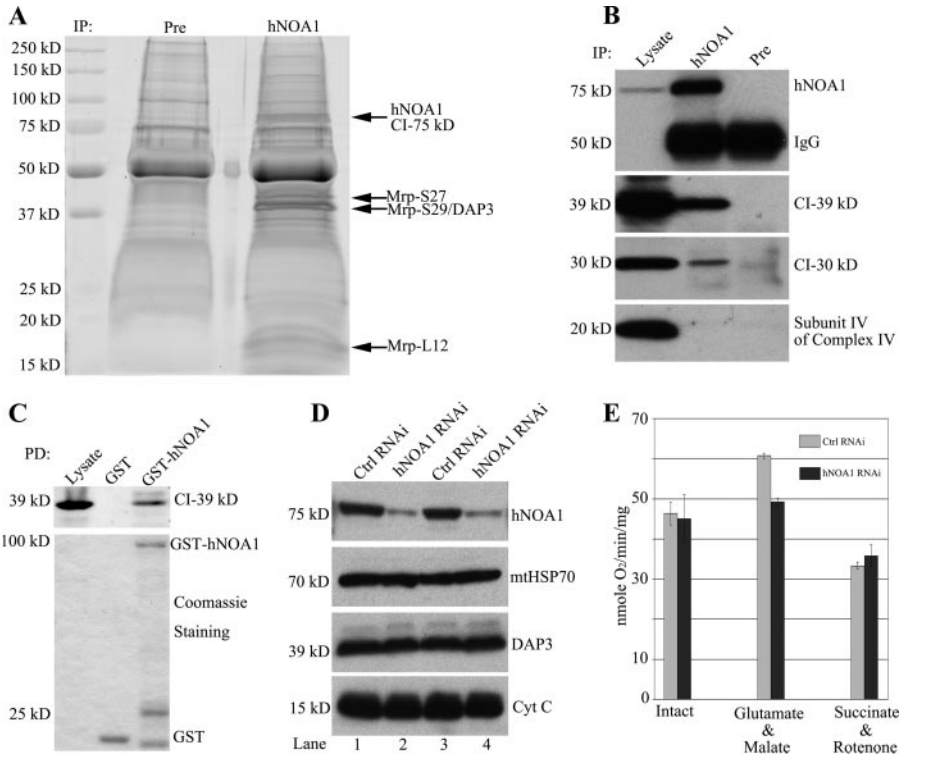

FIGURE 5. **hNOA1 interacts with Complex I of the electron transport chain and regulates NADH-linked mitochondrial O_2 consumption.** *A*, silver-stained gel of immunoprecipitates obtained with anti-hNOA1 or preimmune (*Pre*) IgG. Bands present only in the hNOA1 immunoprecipitates (*arrows*) were identified by mass spectrometry as hNOA1, Complex I, 75 kDa (CI-75 kDa), DAP3/Mrp S29, Mrp S27, and Mrp L12. ~1 mg of enriched mitochondria prepared from HEK293 cells by differential centrifugation were incubated with 40 μg of anti-hNOA1 or preimmune IgG. Immune complexes were bound to 30 μl of protein A-Sepharose beads and separated by 10% SDS-PAGE, followed by silver staining. *B*, hNOA1 coimmunoprecipitates with the 39 kDa (CI-39kD) and 30 kDa (CI-30kD) subunits of Complex I, but not subunit IV of Complex IV. Immunoprecipitates obtained with anti-hNOA1 and preimmune (*Pre*) IgG were separated by SDS-PAGE and immunoblotted for hNOA1, CI-39 kDa, CI-30 kDa and subunit IV of Complex IV. *C*, GST-hNOA1 interacts with the 39-kDa subunit of Complex I in GST-pulldown (*PD*) assays. Immobilized recombinant GST or GST-hNOA1 (~2 μg each) were incubated with HEK293 cell lysates for 4 h, followed by washing with lysis buffer. *Upper panel*, proteins bound to immobilized fusion proteins were eluted with 2× sample buffer for SDS-PAGE and immunoblotted with anti-CI-39 kDa IgG. *Lower panel*, Coomassie Blue staining showing the amount of GST or GST-hNOA1 fusion proteins used for the pulldown assay. *D*, duplicate experiments validating knockdown of hNOA1 expression by hNOA1 siRNA. hNOA1 is depleted ~90% (*lanes 2* and *4*) compared with controls (*lanes 1* and *3*). The amounts of other mitochondrial proteins, such as mtHSP70, DAP3 and cytochrome *c* are similar in control and hNOA1 siRNA-treated samples. HeLa cells (160,000) from control or hNOA1 siRNA-treated samples were lysed directly in 2× sample buffer, followed by SDS-PAGE, and immunoblotting for mitochondrial markers. *E*, knockdown of hNOA1 leads to decreased O_2 consumption in a manner dependent on Complex I, but not Complex II-linked substrates. The rate of O_2 consumption is similar between control and hNOA1 siRNA-treated samples when the cells are either intact or digitonin-permeabilized and supplemented with succinate (plus rotenone). In contrast, the O_2 consumption is reduced ~20% in hNOA1 depleted cells *versus* controls when cells are supplemented with the Complex I-linked substrates, glutamate and malate. 1.0×10^7 intact or digitonin-permeabilized HeLa cells transfected with control or hNOA1 siRNA were suspended in 0.6 ml of KCl medium in the presence of 5 mM glutamate and malate or 5 mM succinate and 2 μM rotenone. The maximal O_2 consumption rates (state 3_u) were measured with a Hansatech Oxytherm electrode by titration with the uncoupler 80 nM carbonyl cyanide *p*-trifluoromethoxyphenylhydrazone.

sion of hNOA1 with doxycycline, mitochondria became small and round in many of the induced cells (Fig. 4, *A–C*), whereas in uninduced cells mostly filamentous mitochondria were seen (Fig. 4, *D–F*). Quantification revealed that ~40% of the induced cells showed small round mitochondria *versus* <5% of the uninduced cells (Fig. 4*G*). No cytochrome *c* release into the cytosol was observed when hNOA1 was induced by addition of doxycycline (Fig. 4, *A–C*). By immunoblotting hNOA1 expression was increased ~3-fold in cells induced with doxycycline compared with those incubated in the absence of doxycycline (Fig. 4*H*).

Next we investigated the effects of depleting hNOA1 on mitochondrial morphology. Transfection of hNOA1 siRNA into COS7 cells led to a decrease of ~90% in the level of hNOA1 expression (Fig. 4*I*). Strikingly, many of the mitochondria in hNOA1 siRNA-transfected cells appeared larger and more swollen (Fig. 4*K*) than mitochondria in control siRNA-transfected cells (Fig. 4*J*). Electron microscopic analysis revealed dramatic changes in the internal organization of the mitochondria especially in the arrangement of the cristae and the density of the mitochondrial matrix when hNOA1 was depleted (Fig. 4, *J–K*). Many of the mitochondria showed a matrix with lower density and simplified, more vesicular cristae than in controls.

Identification of hNOA1 Interaction Partners through IP-MS Analysis—To identify the interacting partners of hNOA1 and gain insights into its mitochondrial functions, we carried out immunoprecipitation with anti-hNOA1 or preimmune IgG on enriched mitochondrial fractions prepared from HEK293 cells. Silver staining of immunoprecipitates revealed that the anti-hNOA1 IgG specifically coimmunoprecipitated four protein bands that were not observed in immunoprecipitates obtained with preimmune serum. By tandem mass spectrometry analysis (Fig. 5*A*), the ~75-kDa band was identified as consisting of both hNOA1 and the 75-kDa subunit of Complex I. Complex I is the first complex of the electron transport chain and spans the IMM with some subunits facing the matrix (36). The two bands at ~40 kDa were identified as DAP3 (also known as Mrp-S29) and Mrp-S27 (mitochondrial ribosomal protein, S27), both of which are localized to the matrix side of the cristae (8, 37). The band at ~17 kDa was identified as Mrp-L12.

hNOA1 Interacts with Complex I and Affects O_2 Consumption in a Complex I-dependent Manner—To confirm the interaction between hNOA1 and Complex I, we performed immunoprecipitation with anti-hNOA1 IgG followed by immunoblotting with antibodies that recognize the 30- and 39-kDa subunits of Complex I. Immunoprecipitated hNOA1 was able to precipitate the 30- and 39-kDa subunits of Complex

I, but not subunit IV of Complex IV (Fig. 5*B*). We were not able to test the association between hNOA1 and the 75-kDa subunit of Complex I in co-immunoprecipitation experiments due to the lack of availability of antibodies commercially. We also confirmed the interaction between hNOA1 and the 39-kDa subunit of Complex I in an *in vitro* GST-hNOA1 pulldown assay. GST-hNOA1, but not GST alone, was able to pull down the 39-kDa subunit of Complex I from HEK293 cell lysates (Fig. 5*C*).

Complex I is the first element of the electron transport chain. It, together with Complex II, receives electrons from NADH or FADH2, respectively, and passes them along the electron transport chain. When ATP is generated by ATP synthase, O_2 is consumed to react with protons and electrons to form H_2O (38). To explore the biological functions of the interaction between hNOA1 and Complex I, we depleted endogenous hNOA1 by siRNA (Fig. 5*D*) and measured O_2 consumption in digitonin-permeabilized HeLa cells (Fig. 5*E*). Glutamate and malate or succinate (plus rotenone) were added to the permeabilized cells as substrates to drive the Complex I- or II-dependent O_2 consumption, respectively (25). After incubation, maximal O_2 consumption rates were measured by titration with the mitochondrial uncoupler carbonyl cyanide *p*-trifluoromethoxyphenylhydrazone with a Hansatech Oxytherm electrode (25). We found that when glutamate and malate were used as substrates the maximal rate of O_2 consumption was reduced ~20% in cells in which hNOA1 was depleted compared with controls (Fig. 5*E*). However, no difference in O_2 consumption was observed between control and hNOA1-depleted cells when cells were intact or supplemented with the Complex II-linked oxidizable substrate, succinate (plus rotenone) (Fig. 5*E*), indicating that hNOA1 regulates the activity of Complex I, but not succinate-dependent respiration. However, succinate-dependent rates or respiration in HeLa cells are uncharacteristically lower than glutamate/malate-dependent rates (39), suggesting rate limitation by other than oxidation at the electron transport chain.

hNOA1 Directly Interacts with DAP3 and Regulates the Cellular Apoptotic Response—In addition to Complex I, we also identified DAP3 as a putative hNOA1 interacting protein from our IP-MS analysis (Fig. 5*A*). We validated the interaction between hNOA1 and DAP3 by co-immunoprecipitation and GST-hNOA1 pulldown assays in which we found that hNOA1 IgG was able to coimmunoprecipitate endogenous DAP3 (Fig. 6*A*), and GST-hNOA1 but not GST alone, was able to pull down DAP3 from HEK293 cell lysates (Fig. 6*B*).

To test whether hNOA1 is able to directly interact with DAP3 we performed pulldown assays with purified recombinant GST-hNOA1 or GST and *in vitro* translated [^{35}S]Met-labeled DAP3 or purified recombinant His_6-tagged DAP3. We found that GST-hNOA1 was able to specifically pull down both [^{35}S]Met-DAP3 (Fig. 6*C*) and His_6-DAP3 (Fig. 6*D*). Collectively, these results indicate that hNOA1 is able to directly interact with DAP3.

DAP3 was first identified as a positive regulator for γ-interferon-mediated apoptosis, because inactivation of DAP3 by antisense RNA protected cells from γ-interferon-induced cell death (10). To determine whether knockdown of hNOA1 has a similar effect we carried out a cell viability assay in the presence

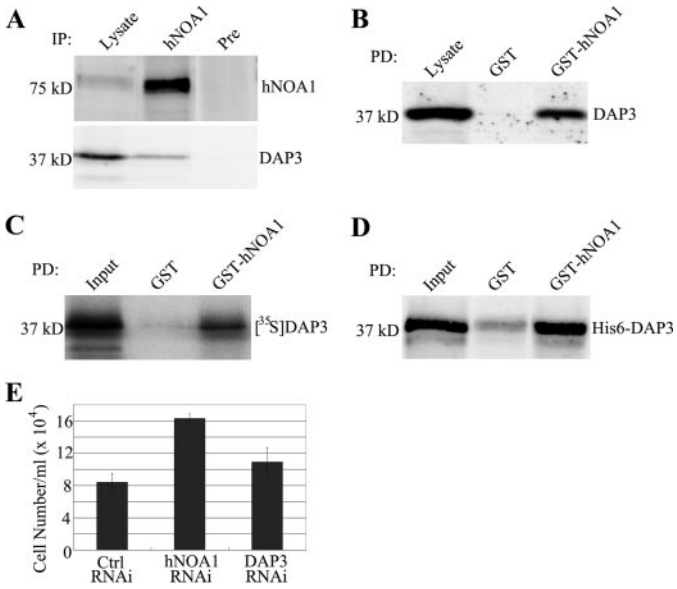

FIGURE 6. **hNOA1 directly interacts with DAP3 and regulates γ-interferon induced apoptosis.** *A*, hNOA1 coimmunoprecipitates with endogenous DAP3. Immunoprecipitates obtained from equal aliquots of HEK293 cell lysates with anti-hNOA1 and preimmune (*Pre*) IgG were separated by SDS-PAGE and immunoblotted with antibodies against hNOA1 and DAP3. *B*, GST-hNOA1 but not GST alone specifically interacts with endogenous DAP3 from HEK293 cells in GST-pulldown assays. Pulldown assays were carried out as in Fig. 5*C*. *C*, *in vitro* translated, [^{35}S]Met-labeled DAP3 binds to GST-hNOA1, but not GST alone. GST-hNOA1 and GST alone (~2 μg each) immobilized on glutathione beads were incubated with *in vitro* translated DAP3. Bound proteins were separated by SDS-PAGE and detected by autoradiography. *D*, GST-hNOA1 but not GST alone, interacts with purified His_6-DAP3. GST-hNOA1 and GST alone (~2 μg each) immobilized on glutathione beads were incubated with ~200 ng of recombinant His_6-DAP3 purified from *E. coli*. Bound proteins were separated by SDS-PAGE, followed by immunoblotting with anti-DAP3 IgG. *E*, depletion of hNOA1 or DAP3 renders cells more resistant to γ-interferon-induced apoptosis. HeLa cells were plated and transfected with control, hNOA1, or DAP3 siRNA and placed in fresh DMEM containing 1000 units/ml γ-interferon. 2.5 days later, cells were trypsinized and collected in 1 ml of fresh DMEM and counted using a Vi-Cell cell counter (Beckman Coulter).

of γ-interferon. We found that twice as many hNOA1-depleted HeLa cells survived than controls in the presence of γ-interferon and more survived compared with DAP3-depleted cells (Fig. 6*E*), suggesting depletion of hNOA1 protects cells from γ-interferon-mediated apoptosis.

hNOA1 Knockdown Protects Cells from Staurosporine-induced Apoptosis—DAP3 was also reported to be involved in staurosporine-induced mitochondrial fragmentation (11), which leads to apoptosis, and recently it was also found that overexpression of the mouse homologue of hNOA1, mAtNOS1, leads to apoptosis in human neuroblastoma cells and human mammary adenocarcinoma cells (40, 41). To examine whether hNOA1 affects staurosporine-induced apoptosis, HeLa cells transfected with control or hNOA1 siRNA were treated with staurosporine (for 5 h), followed by detection of *in situ* cell death by TUNEL staining. We found that cells transfected with hNOA1 siRNA (Fig. 7, *C* and *D*) showed less prominent TUNEL staining after staurosporine treatment than those transfected with control siRNA (Fig. 7, *A* and *B*). Quantification revealed that 45% of the hNOA1-depleted cells showed TUNEL staining compared with 72% of controls (Fig. 7*E*). Besides TUNEL staining, we also examined cytochrome *c* release, a hallmark of staurosporine-induced apoptosis. Without stauro-

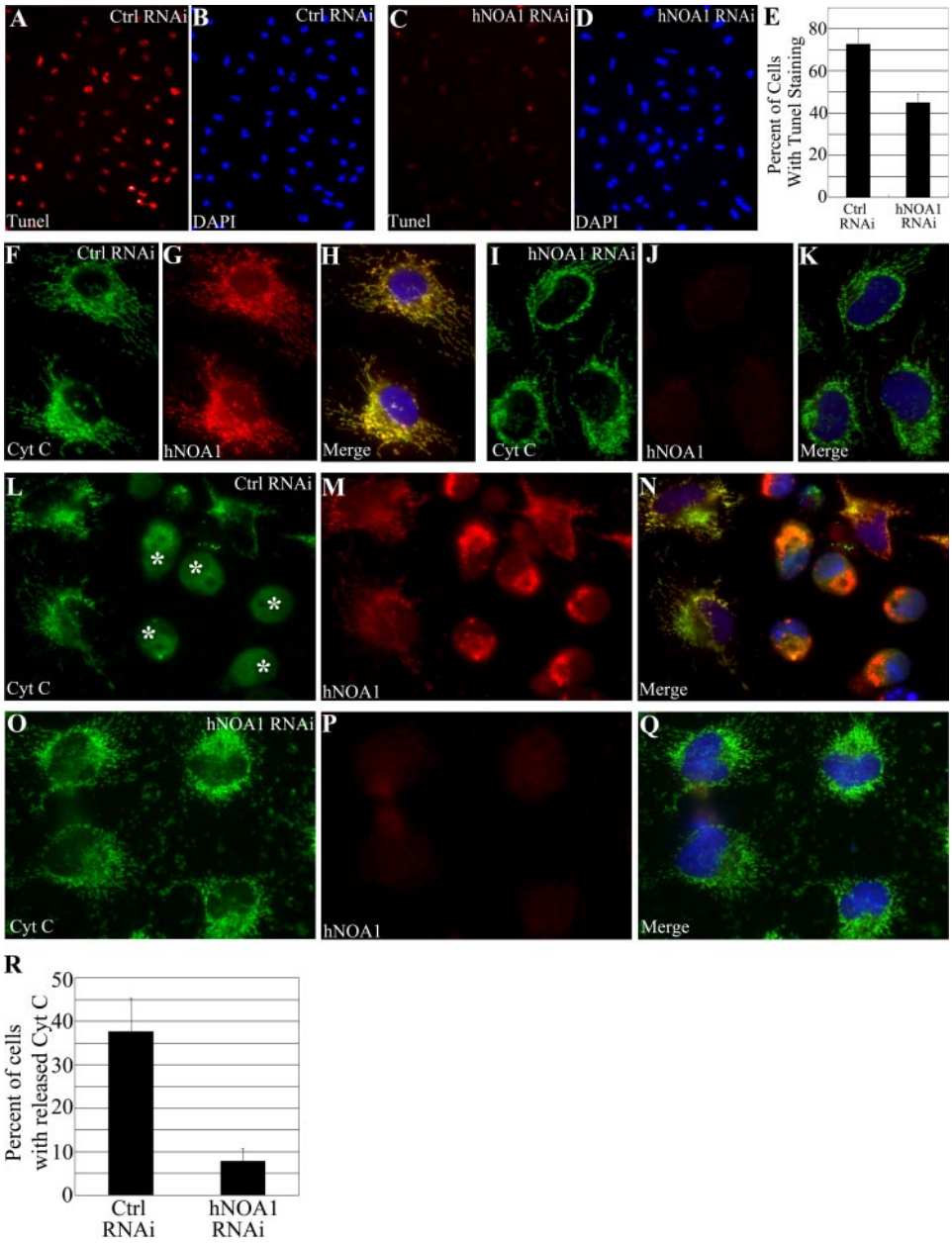

FIGURE 7. **hNOA1 knockdown protects cells from staurosporine-induced apoptosis.** HeLa cells transfected with control siRNA (*A* and *B*) or hNOA1 siRNA (*C* and *D*) for 3 days were treated with 2 μM staurosporine for 5 h after which cells were fixed in 2% PFA, followed by TUNEL staining (*red* nuclear staining in *A* and *C*) to detect apoptotic cells and 4′,6-diamidino-2-phenylindole staining (*DAPI*) (*B* and *D*). Fewer cells show TUNEL staining in hNOA1-depleted cells then in controls (compare *A* and *C*). *E*, quantification reveals that cells transfected with hNOA1 siRNA (*hNOA1 RNAi*) show ~30% less TUNEL staining than those transfected with control siRNA. For either control or hNOA1 siRNA transfected samples total cells (595 for *ctrl RNAi*; 493 for *hNOA1 RNAi*), and apoptotic cells were counted in eight randomly selected fields based on 4′,6-diamidino-2-phenylindole and TUNEL staining, respectively. *F–K*, cytochrome *c* release is not observed in HeLa cells transfected with either control or hNOA1 siRNA in the absence of staurosporine. *L–Q*, in control siRNA-transfected samples treated with staurosporine more cells in which cytochrome *c* has been released (*asterisk* in *L*) are observed than in hNOA1 siRNA-transfected samples (*O*). HeLa cells transfected with control (*L–N*) or hNOA1 (*O* and *P*) siRNA for 3 days were treated or not with staurosporine as above and processed for double immunofluorescence with anti-Cyt C (*L* and *O*) and anti-hNOA1 (*M* and *P*) IgG. *R*, quantification reveals that only ~7% of the cells transfected with hNOA1 siRNA (*hNOA1 RNAi*) showed cytochrome *c* release, whereas ~37% of the cells transfected with control siRNA (*ctrl RNAi*) showed cytochrome *c* release. For either control or hNOA1 siRNA-transfected samples, eight fields were randomly selected, and the total number of cells (420 for *ctrl RNAi*; 316 for *hNOA1 RNAi*), and the percentage of the total with released cytochrome *c* was counted.

sporine treatment, no release of cytochrome *c* was observed by immunofluorescence in either controls (Fig. 7, *F–H*) or hNOA1 (Fig. 7, *I–K*)-depleted cells. By contrast, after staurosporine treatment ~37% of the control siRNA-transfected cells showed cytochrome *c* release into the cytoplasm (Fig. 7, *L–N*), whereas ~7% of hNOA1 siRNA-transfected cells showed cytochrome *c* release (Fig. 7, *O–R*). Furthermore, we observed that mitochondria became small and round in control siRNA-transfected cells upon staurosporine treatment as previously reported by others (42). Interestingly, when hNOA1 was down-regulated by siRNA this morphological change was delayed compared with that in control siRNA-transfected cells. After prolonged treatment (>6 h) the mitochondria became small and round, released cytochrome *c* and became apoptotic. We conclude that depletion of hNOA1 partially protects cells from staurosporine-induced apoptosis.

DISCUSSION

In this study we localized endogenous hNOA1 by immunoelectron microscopy and mitochondrial subfractionation, established its presence in mitochondria, and demonstrated that it is peripherally associated with the IMM facing the matrix. We also identified two novel interacting partners of hNOA1 through IP-MS analysis. Endogenous hNOA1 was found to interact with both Complex I of the electron transport chain and DAP3, a protein involved in apoptosis. siRNA depletion of hNOA1 led to a decrease in mitochondrial O_2 consumption in a Complex I-dependent manner and made cells less susceptible to γ-interferon and staurosporine-induced apoptosis, suggesting a functional link between hNOA1, Complex I, and DAP3. Thus hNOA1 plays a role in regulating both mitochondrial respiration and apoptosis.

The *Arabidopsis* homologue of hNOA1 was first identified as a putative mitochondrial nitric-oxide synthase (NOS) (26), but neither the AtNOS1/AtNOA1 fusion protein or its homologues were found to have NOS activity (28). Based on the finding that the AtNOA1 mutant showed impaired NO synthesis (26), it is possible that AtNOA1 might associate with other unknown proteins to reg-

ulate NO production. It was speculated that one of the candidates could be a component of the mitochondrial electron transport system (30). More recently, activation of Complex I of the electron transport chain by NADH or its inactivation by rotenone has been suggested to regulate mitochondrial NOS activity (43, 44); however, this point has proved to be controversial (45). It is conceivable that Complex I might couple to NAD(P)H to accept electrons that can be used for mitochondrial NOS to produce NO. Our findings, showing that hNOA1 is in the same complex with Complex I, raise the interesting possibility that Complex I activity might affect NO production through hNOA1. Alternatively, hNOA1 might regulate Complex I activity. Indeed, we obtained evidence showing that depletion of hNOA1 leads to decreased Complex I-dependent O_2 consumption.

Overexpression of hNOA1 led to the formation of small, round mitochondria, whereas depletion of hNOA1 led to enlarged mitochondria with abnormal cristae. The effects of hNOA1 overexpression and depletion on mitochondrial morphology are similar to those observed when mitochondrial fission proteins such as Drp1 or Fis1 are perturbed (46, 47), suggesting that hNOA1 might play a role in mitochondrial fission. Two other large G proteins, Mfn1(2)/fuzzy onions 1 and 2, are responsible for the fusion of the OMM (48), and Opa1/Mgm1P is responsible for the fusion of the IMM (49). Drp1/Dnm1 is responsible for the fission of the OMM (33, 50), but no large G protein has yet been identified that is involved in fission of the IMM. It is possible that hNOA1 might be the large G protein that facilitates fission of the IMM. Our finding that depletion of hNOA1 also makes cells less susceptible to apoptotic stimuli, such as staurosporine, is consistent with results obtained after knockdown of other fission proteins, such as Drp1 or Fis1 (42).

In addition to its interaction with Complex I, we demonstrated that hNOA1 directly interacts with DAP3, and depletion of hNOA1 protects cells from apoptosis. Whether the interaction is sufficient to mediate the role of hNOA1 in apoptosis remains to be elucidated. Besides its role in apoptosis, we also showed that depletion of hNOA1 affects mitochondrial respiration in a Complex I-dependent manner. One explanation for hNOA1's dual roles in both respiration and apoptosis is its interaction with DAP3. Interestingly, DAP3 was identified as a component of mitochondrial ribosomes (37, 51, 52), which are responsible for synthesis of the 13 proteins encoded by the mitochondrial genome (53). 7 of the 13 proteins synthesized by mitochondrial ribosomes are Complex I subunits of the electron transport chain (53), and we identified not only Complex I, but also two additional ribosome proteins, Mrp-S27 and Mrp-L12, as interacting partners of hNOA1 by IP-MS. We confirmed the interaction of NOA1 with endogenous Mrp-S27 in co-immunoprecipitation and pull-down assays on HEK293 cell lysates (supplemental Fig. S1, *A* and *B*). It will be interesting to determine if hNOA1 can regulate ribosomal functions in synthesizing mitochondrial encoded proteins either through its interaction with DAP3 or other mitochondrial ribosomal proteins such as Mrp-S27 and Mrp-L12, identified from our IP-MS analysis. This will provide additional information on how hNOA1 affects these processes, and how different mitochondrial functions coordinate with each other overall.

It is of interest that point mutations in the seven mitochondrial encoded Complex I genes have been shown to cause defects in Complex I assembly and activity (54), which leads to serious diseases, such as Leber hereditary optic neuropathy (55) or mitochondrial encephalopathy (56). Defects in Complex I assembly and activity can also lead to alterations in mitochondrial morphology (57).

Mitochondrial respiration, apoptosis, and dynamics are intimately intertwined (2). It is conceivable that proteins involved in these three different mitochondrial processes communicate with each other to maintain the multiple functions of this important organelle. Our characterization of the multifunctional roles of hNOA1 and its interaction with both Complex I and DAP3 suggest that hNOA1 could play a role in coordinating these processes. Further investigations are needed to better understand how hNOA1 is involved in each process mechanistically, how GTP binding affects these processes, and how different mitochondrial functions coordinate with each other overall.

Acknowledgment—We thank Dr. Sandy Wiley for assistance with mitochondrial purification.

REFERENCES

1. Bossy-Wetzel, E., Barsoum, M. J., Godzik, A., Schwarzenbacher, R., and Lipton, S. A. (2003) *Curr. Opin. Cell Biol.* **15,** 706–716
2. McBride, H. M., Neuspiel, M., and Wasiak, S. (2006) *Curr. Biol.* **16,** R551–R560
3. Chan, D. C. (2006) *Annu. Rev. Cell Dev. Biol.* **22,** 79–99
4. Olichon, A., Baricault, L., Gas, N., Guillou, E., Valette, A., Belenguer, P., and Lenaers, G. (2003) *J. Biol. Chem.* **278,** 7743–7746
5. Chen, H., Chomyn, A., and Chan, D. C. (2005) *J. Biol. Chem.* **280,** 26185–26192
6. Jin, Z., and El-Deiry, W. S. (2005) *Cancer Biol. Ther.* **4,** 139–163
7. Kim, R., Emi, M., and Tanabe, K. (2006) *Cancer Chemother. Pharmacol.* **57,** 545–553
8. Berger, T., Brigl, M., Herrmann, J. M., Vielhauer, V., Luckow, B., Schlondorff, D., and Kretzler, M. (2000) *J. Cell Sci.* **113,** 3603–3612
9. Kim, H. R., Chae, H. J., Thomas, M., Miyazaki, T., Monosov, A., Monosov, E., Krajewska, M., Krajewski, S., and Reed, J. C. (2007) *FASEB J.* **21,** 188–196
10. Kissil, J. L., Deiss, L. P., Bayewitch, M., Raveh, T., Khaspekov, G., and Kimchi, A. (1995) *J. Biol. Chem.* **270,** 27932–27936
11. Mukamel, Z., and Kimchi, A. (2004) *J. Biol. Chem.* **279,** 36732–36738
12. Alberts, B., Bray, D., Lewis, J., Raff, M., Roberts, K., and Walter, P. (2008) *Mol. Biol. Cell* **5,** 827–840
13. Crawford, N. M., Galli, M., Tischner, R., Heimer, Y. M., Okamoto, M., and Mack, A. (2006) *Trends Plant Sci.* **11,** 526–527
14. Lin, P., Le-Niculescu, H., Hofmeister, R., McCaffery, J. M., Jin, M., Hennemann, H., McQuistan, T., De Vries, L., and Farquhar, M. G. (1998) *J. Cell Biol.* **141,** 1515–1527
15. Nagai, M., Meerloo, T., Takeda, T., and Farquhar, M. G. (2003) *Mol. Biol. Cell* **14,** 4984–4996
16. Le-Niculescu, H., Niesman, I., Fischer, T., DeVries, L., and Farquhar, M. G. (2005) *J. Biol. Chem.* **280,** 22012–22020
17. Fukushima, N. H., Brisch, E., Keegan, B. R., Bleazard, W., and Shaw, J. M. (2001) *Mol. Biol. Cell* **12,** 2756–2766
18. Morimoto, T., Loh, P. C., Hirai, T., Asai, K., Kobayashi, K., Moriya, S., and Ogasawara, N. (2002) *Microbiology* **148,** 3539–3552
19. Zheng, B., Lavoie, C., Tang, T. D., Ma, P., Meerloo, T., Beas, A., and Farquhar, M. G. (2004) *Mol. Biol. Cell* **15,** 5538–5550

20. Lapidus, R. G., and Sokolove, P. M. (1993) *Arch Biochem. Biophys.* **306,** 246–253
21. Pagliarini, D. J., Wiley, S. E., Kimple, M. E., Dixon, J. R., Kelly, P., Worby, C. A., Casey, P. J., and Dixon, J. E. (2005) *Mol. Cell* **19,** 197–207
22. Wiley, S. E., Murphy, A. N., Ross, S. A., van der Geer, P., and Dixon, J. E. (2007) *Proc. Natl. Acad. Sci. U. S. A.* **104,** 5318–5323
23. Zhou, W., Ryan, J. J., and Zhou, H. (2004) *J. Biol. Chem.* **279,** 32262–32268
24. Lehtonen, S., Shah, M., Nielsen, R., Iino, N., Ryan, J. J., Zhou, H., and Farquhar, M. G. (2008) *Mol. Biol. Cell* **19,** 2949–2961
25. Murphy, A. N., Bredesen, D. E., Cortopassi, G., Wang, E., and Fiskum, G. (1996) *Proc. Natl. Acad. Sci. U. S. A.* **93,** 9893–9898
26. Guo, F. Q., Okamoto, M., and Crawford, N. M. (2003) *Science* **302,** 100–103
27. Huang, S., Kerschbaum, H. H., Engel, E., and Hermann, A. (1997) *J. Neurochem.* **69,** 2516–2528
28. Zemojtel, T., Frohlich, A., Palmieri, M. C., Kolanczyk, M., Mikula, I., Wyrwicz, L. S., Wanker, E. E., Mundlos, S., Vingron, M., Martasek, P., and Durner, J. (2006) *Trends Plant Sci.* **11,** 524–525; author reply 526–528
29. Moreau, M., Lee, G. I., Wang, Y., Crane, B. R., and Klessig, D. F. (2008) *J. Biol. Chem.* **283,** 32957–32967
30. Zemojtel, T., Kolanczyk, M., Kossler, N., Stricker, S., Lurz, R., Mikula, I., Duchniewicz, M., Schuelke, M., Ghafourifar, P., Martasek, P., Vingron, M., and Mundlos, S. (2006) *FEBS Lett.* **580,** 455–462
31. Hobman, T. C., Zhao, B., Chan, H., and Farquhar, M. G. (1998) *Mol. Biol. Cell* **9,** 1265–1278
32. Eskelinen, E. L., Schmidt, C. K., Neu, S., Willenborg, M., Fuertes, G., Salvador, N., Tanaka, Y., Lullmann-Rauch, R., Hartmann, D., Heeren, J., von Figura, K., Knecht, E., and Saftig, P. (2004) *Mol. Biol. Cell* **15,** 3132–3145
33. Bleazard, W., McCaffery, J. M., King, E. J., Bale, S., Mozdy, A., Tieu, Q., Nunnari, J., and Shaw, J. M. (1999) *Nat. Cell Biol.* **1,** 298–304
34. Cortese, J. D., Voglino, A. L., and Hackenbrock, C. R. (1995) *Biochim. Biophys. Acta* **1228,** 216–228
35. Satoh, M., Hamamoto, T., Seo, N., Kagawa, Y., and Endo, H. (2003) *Biochem. Biophys. Res. Commun.* **300,** 482–493
36. Lenaz, G., Fato, R., Genova, M. L., Bergamini, C., Bianchi, C., and Biondi, A. (2006) *Biochim. Biophys. Acta* **1757,** 1406–1420
37. Suzuki, T., Terasaki, M., Takemoto-Hori, C., Hanada, T., Ueda, T., Wada, A., and Watanabe, K. (2001) *J. Biol. Chem.* **276,** 33181–33195
38. Hatefi, Y. (1985) *Annu. Rev. Biochem.* **54,** 1015–1069
39. Vrbacky, M., Krijt, J., Drahota, Z., and Melkova, Z. (2003) *Physiol. Res.* **52,** 545–554
40. Parihar, M. S., Parihar, A., Chen, Z., Nazarewicz, R., and Ghafourifar, P. (2008) *Biochim. Biophys. Acta* **1780,** 921–926
41. Parihar, A., Parihar, M. S., Chen, Z., and Ghafourifar, P. (2008) *Life Sci.* **82,** 1077–1082
42. Lee, Y. J., Jeong, S. Y., Karbowski, M., Smith, C. L., and Youle, R. J. (2004) *Mol. Biol. Cell* **15,** 5001–5011
43. Parihar, M. S., Nazarewicz, R. R., Kincaid, E., Bringold, U., and Ghafourifar, P. (2008) *Biochem. Biophys. Res. Commun.* **366,** 23–28
44. Parihar, M. S., Parihar, A., Villamena, F. A., Vaccaro, P. S., and Ghafourifar, P. (2008) *Biochem. Biophys. Res. Commun.* **367,** 761–767
45. Venkatakrishnan, P., Nakayasu, E. S., Almeida, I. C., and Miller, R. T. (2008) *Faseb. J.* **22,** 835
46. Tondera, D., Czauderna, F., Paulick, K., Schwarzer, R., Kaufmann, J., and Santel, A. (2005) *J. Cell Sci.* **118(Pt 14),** 3049–3059
47. Jofuku, A., Ishihara, N., and Mihara, K. (2005) *Biochem. Biophys. Res. Commun.* **333,** 650–659
48. Santel, A., and Fuller, M. T. (2001) *J. Cell Sci.* **114(Pt 5),** 867–874
49. Meeusen, S., DeVay, R., Block, J., Cassidy-Stone, A., Wayson, S., McCaffery, J. M., and Nunnari, J. (2006) *Cell* **127,** 383–395
50. Frank, S., Gaume, B., Bergmann-Leitner, E. S., Leitner, W. W., Robert, E. G., Catez, F., Smith, C. L., and Youle, R. J. (2001) *Dev. Cell* **1,** 515–525
51. Cavdar Koc, E., Ranasinghe, A., Burkhart, W., Blackburn, K., Koc, H., Moseley, A., and Spremulli, L. L. (2001) *FEBS Lett.* **492,** 166–170
52. Sudhamsu, J., Lee, G. I., Klessig, D. F., and Crane, B. R. (2008) *J. Biol. Chem.* **283,** 32968–32976
53. Anderson, S., Bankier, A. T., Barrell, B. G., de Bruijn, M. H., Coulson, A. R., Drouin, J., Eperon, I. C., Nierlich, D. P., Roe, B. A., Sanger, F., Schreier, P. H., Smith, A. J., Staden, R., and Young, I. G. (1981) *Nature* **290,** 457–465
54. Cardol, P., Matagne, R. F., and Remacle, C. (2002) *J. Mol. Biol.* **319,** 1211–1221
55. DiMauro, S. (2001) *Semin. Cell Dev. Biol.* **12,** 397–405
56. Malfatti, E., Bugiani, M., Invernizzi, F., de Souza, C. F., Farina, L., Carrara, F., Lamantea, E., Antozzi, C., Confalonieri, P., Sanseverino, M. T., Giugliani, R., Uziel, G., and Zeviani, M. (2007) *Brain* **130(Pt 7),** 1894–1904
57. Koopman, W. J., Visch, H. J., Verkaart, S., van den Heuvel, L. W., Smeitink, J. A., and Willems, P. H. (2005) *Am. J. Physiol. Cell Physiol.* **289,** C881–890